

Fermi National Accelerator Laboratory

FERMILAB-Pub-92/153

E687

**Study of $D^0 \rightarrow K^0_S \pi^+ \pi^-$ and $D^0 \rightarrow K^0_S K^+ K^-$ in
High Energy Photoproduction**

E687 Collaboration

*Fermi National Accelerator Laboratory
P.O. Box 500, Batavia, Illinois 60510*

June 1992

Submitted to *Physics Letters*

Disclaimer

This report was prepared as an account of work sponsored by an agency of the United States Government. Neither the United States Government nor any agency thereof, nor any of their employees, makes any warranty, express or implied, or assumes any legal liability or responsibility for the accuracy, completeness, or usefulness of any information, apparatus, product, or process disclosed, or represents that its use would not infringe privately owned rights. Reference herein to any specific commercial product, process, or service by trade name, trademark, manufacturer, or otherwise, does not necessarily constitute or imply its endorsement, recommendation, or favoring by the United States Government or any agency thereof. The views and opinions of authors expressed herein do not necessarily state or reflect those of the United States Government or any agency thereof.

Study of $D^0 \rightarrow K_S^0 \pi^+ \pi^-$ and $D^0 \rightarrow K_S^0 K^+ K^-$
in High Energy Photoproduction

P.L. Frabetti

Dip. di Fisica dell'Università and INFN - Bologna, I-40126 Bologna, Italy

C.W. Bogart[a], H.W.K. Cheung, S. Culy, J.P. Cumalat

University of Colorado, Boulder, CO 80309, USA

J.N. Butler, F. Davenport[b], I. Gaines, P.H. Garbincius, S. Gourlay, D.J. Harding,

P. Kasper, A. Kreymer, P. Lebrun, H. Mendez[c]

Fermilab, Batavia, IL 60510, USA

S. Bianco, M. Enorini, F.L. Fabbri, A. Spallone, A. Zallo

Laboratori Nazionali di Frascati dell'INFN, I-00044 Frascati, Italy

R. Culbertson, G. Jaross[d], K. Lingel[e], P.D. Sheldon[f], J.R. Wilson[g], J. Wiss

University of Illinois at Urbana-Champaign, Urbana, IL 61801, USA

G. Alimonti, G. Bellini, M. Di Corato, M. Giammarchi, F. Leveraro, S. Malvezzi,

D. Menasce, E. Meroni, L. Moroni, D. Pedrini, L. Perasso, A. Sala, S. Sala,

D. Torretta[h], M. Vittone[h]

Dip. di Fisica dell'Università and INFN - Milano, I-20133 Milan, Italy

D. Buchholz, C. Castoldi[i], B. Gobbi, S. Park[h], R. Yoshida[j]

Northwestern University, Evanston, IL 60208, USA

J.M. Bishop, J.K. Busenitz[k], N.M. Cason, J.D. Cunningham[l], R.W. Gardner[m],

C.J. Kennedy, E.J. Mannel[n], R.J. Mountain, D.L. Puseljic, R.C. Ruchti,

W.D. Shephard, M.E. Zanabria

University of Notre Dame, Notre Dame, IN 46556, USA

G. Boca, S.P. Ratti, P. Vitulo

Dip. di Fisica Nucleare dell'Università and INFN - Pavia, I-27100 Pavia, Italy

A. Lopez

University of Puerto Rico at Mayaguez, Puerto Rico

Analysis of the resonant and non-resonant branching fractions for the decays $D^0 \rightarrow K_S^0 \pi^+ \pi^-$ and $D^0 \rightarrow K_S^0 K^+ K^-$ is presented. For the $D^0 \rightarrow K_S^0 \pi^+ \pi^-$ decay, a fit to the observed Dalitz plot was performed to determine the complex amplitudes of the sub-component modes. For the $D^0 \rightarrow K_S^0 K^+ K^-$ decay, measurements of the branching ratios $D^0 \rightarrow K_S^0 K^+ K^-$ (inclusive), $D^0 \rightarrow K_S^0 \phi$, and $D^0 \rightarrow K_S^0 (K^+ K^-)_{non-\phi}$ relative to the $D^0 \rightarrow K_S^0 \pi^+ \pi^-$ mode are reported. The data were collected by the Fermilab high energy photoproduction experiment E687.

Theoretical models[1] have been developed to explain weak decay mechanisms of D mesons. Most of these models require experimentally measured branching ratios and deal only with the two-body decays. Several experiments¹ have provided data to investigate three-body final states of D mesons and to determine the exclusive rates into resonant two-body channels. In this paper we report measurements of the resonant and non-resonant branching fractions of the decays $D^0 \rightarrow K_S^0 \pi^+ \pi^-$ and $D^0 \rightarrow K_S^0 K^+ K^-$ from the Fermilab high energy photoproduction experiment E687.

The E687 detector, which is described in detail elsewhere[7], is a large aperture multiparticle spectrometer with good detection capabilities for charged hadrons and photons. A microvertex detector consisting of 12 planes of silicon microstrips arranged in three views provides high resolution tracking allowing the separation of primary and secondary vertices. Deflections of charged particles by two analysis magnets of opposite polarity are measured by five stations of multiwire proportional chambers (PWCs). Three multicell Čerenkov counters operating in threshold mode are used for particle identification. The photon beam is derived from a 350 GeV/c electron beam with a $\sigma = 13\%$ momentum spread. The electron beam impinges on a 27% radiation length lead foil producing bremsstrahlung photons. The photons are directed to a 4 cm long Be target.² The experimental trigger required that at least 35 GeV of energy be deposited in the hadron calorimeter; that at least two tracks be present outside of the region where Bethe-Heitler pairs are produced; and that the radiated energy loss between the recoil and incident electrons exceeded 130 GeV. The average photon energy for the data sample was 221 GeV. In this analysis, neutral kaons were detected via the decay mode $K_S^0 \rightarrow \pi^+ \pi^-$ in a volume ranging from the experimental

¹For example, see Refs.[2-6].

²Approximately 13% of the data was taken with a Si - Be composite target.

target to the first PWC station[7]. From the full 1987-88 data sample of 6×10^7 triggers, approximately 10^6 K_S^0 candidates were reconstructed.³

The analysis of the decay $D^0 \rightarrow K_S^0 \pi^+ \pi^-$ proceeded as follows. Pairs of oppositely charged tracks were combined with a K_S^0 candidate to form a D^0 candidate. The pion candidates from the D^0 vertex were required to have Čerenkov light patterns consistent with the pion hypothesis. These tracks, together with the K_S^0 candidate, were tested to form a common secondary vertex with a confidence level exceeding 1%. A search for the primary vertex was made using a “seed” track reconstructed from the D^0 candidate momentum vector and the secondary vertex point. Remaining tracks in the event were intersected with the seed track so long as the confidence level of the resultant vertex exceeded 2%. An acceptable primary vertex candidate was required to have at least three tracks including the seed track. In addition, the D^0 candidate momentum was restricted to the range $45 < P(D^0) < 160$ GeV/c, corresponding to the region of good acceptance by the spectrometer. To reject background, the secondary vertex was required to be separated from the primary vertex by a decay flight distance⁴ $\ell > 10\sigma_\ell$. The invariant mass spectrum for $D^0 \rightarrow K_S^0 \pi^+ \pi^-$ candidates satisfying these cuts is shown in Fig. 1. Superimposed on the histogram is a curve consisting of a Gaussian function for the signal and a linear background. The yield of events in the signal peak is 137 ± 19 and the central mass value of 1.862 ± 0.002 GeV/c² is consistent with the accepted value[8]. This sample was used as a reference mode for the $D^0 \rightarrow K_S^0 K^+ K^-$ analysis.

³The reconstructed $\pi^+ \pi^-$ invariant mass was required to be within either 5σ or ± 20 MeV/c² of the accepted[8] K_S^0 mass value.

⁴The variable ℓ is the signed 3 dimensional separation between vertices and σ_ℓ is the error on ℓ computed on an event by event basis including effects of multiple coulomb scattering.

For the Dalitz plot analysis of $D^0 \rightarrow K_S^0 \pi^+ \pi^-$, additional secondary vertex isolation cuts were employed to enhance the signal to background ratio. Leftover tracks not found in the primary vertex were required to be inconsistent with emerging from the secondary vertex, and secondary tracks were required not to point to the primary vertex. Candidates passing these additional cuts are shown in Fig. 2 in which the fitted yield was determined to be 114 ± 13 .

A maximum likelihood fit to the Dalitz plot was used to measure the decay fractions into the modes $K^{*-} \pi^+$, $\bar{K}^0 \rho^0$, and three-body non-resonant. Combinations having $K_S^0 \pi^+ \pi^-$ invariant mass within 1.5σ of the D^0 were selected for the analysis. Since the charm quantum number of the observed state is not determined by the K_S^0 , the data were fit to an average of D^0 and \bar{D}^0 amplitudes. The D^0 decay is specified in terms of amplitude coefficients a_1, a_3 , and phases δ_1, δ_3 by

$$\mathcal{A}(D^0) = a_1 e^{i\delta_1} + B(K_S^0 \pi^- \pi^+ | K^*) + a_3 e^{i\delta_3} B(\pi^+ \pi^- K_S^0 | \rho^0) \quad (1)$$

where attention should be given to the order of particle labels. Here B represents a complex Breit-Wigner function⁵ which describes the strong resonances and decay angular momentum conservation:

$$B(a b c | r) = -2 \vec{c} \cdot \vec{a} \frac{\sqrt{M_r \Gamma}}{M_r^2 - M_{ab}^2 - i \Gamma M_r}. \quad (2)$$

The \vec{c} and \vec{a} are three momenta of particles c and a measured in the ab rest frame. For the \bar{D}^0 decay, the amplitude is specified by

$$\mathcal{A}(\bar{D}^0) = a_1 e^{i\delta_1} + B(K_S^0 \pi^+ \pi^- | K^*) + a_3 e^{i\delta_3} B(\pi^- \pi^+ K_S^0 | \rho^0). \quad (3)$$

To account for background, an average of high and low D^0 sideband fits reflecting a flat non-resonant term with uniformly populated $K^{*\pm}$ bands was used. The amplitudes

⁵For each resonance of mass M_r we use a width Γ which is proportional to p^3 where p is the decay momentum in the resonance rest frame.

are weighted by a function to correct for geometrical acceptance and reconstruction efficiency; effects due to finite mass resolution by the spectrometer were proven to be negligible. A likelihood function consisting of signal and background probability densities was maximized over the variables $a_1, \delta_1, a_3, \delta_3$. An additional term is added to the likelihood in order to tie the background level in the signal region to the level expected from the $K_S^0\pi^+\pi^-$ mass sidebands.⁶

The Dalitz plot, mass-squared projections, and fit results are illustrated in Fig. 3. In Table I the fitted parameters are given with statistical errors only. In Table II the decay fractions are compared to results from the Mark III experiment[6].⁷ The decay fraction into a given mode was computed by integrating the signal intensity with the amplitudes for all other modes zeroed divided by the integrated intensity with all modes present. These fractions do not sum to one due to the presence of interference between the modes. The systematic errors in the decay fractions reflect uncertainties in reconstruction efficiency and background parameterization.⁸

The analysis of the decay $D^0 \rightarrow K_S^0 K^+ K^-$ proceeded in much the same fashion as that for $D^0 \rightarrow K_S^0 \pi^+ \pi^-$ with two exceptions. First, using the Čerenkov information,

⁶The additional term is the logarithm of the Gaussian probability for finding the observed signal fraction given the expected value and error from a fit to the $K_S^0\pi^+\pi^-$ mass spectrum.

⁷While comparing our phase conventions with those of Ref.[6], a mistake was found in the charm symmetrization of their $K_S^0\pi^+\pi^-$ amplitude (private communication). We therefore choose not to make a comparison of phases.

⁸The systematic uncertainty due to reconstruction efficiency was estimated by using functions derived from different Monte Carlo data sets and smoothing techniques. The systematic uncertainty due to background parameterization was estimated by varying the background K^* fraction and by allowing the possibility of background ρ production.

the charged kaons emerging from the D^0 decay vertex were required to be consistent with the kaon hypothesis. Second, the secondary decay flight was required to satisfy $\ell/\sigma_\ell > 2$. Combinations satisfying these cuts are histogrammed in Fig. 4. The D^0 yield from the fit shown is 47 ± 12 events.

Relative branching ratio measurements for the decays $D^0 \rightarrow K_S^0 K^+ K^-$ (inclusive), $D^0 \rightarrow K_S^0 \phi$, and $D^0 \rightarrow K_S^0 (K^+ K^-)_{non-\phi}$ were made relative to the $D^0 \rightarrow K_S^0 \pi^+ \pi^-$ decay mode because of its larger branching ratio and similar decay topology. Corrections due to track, vertex and K_S^0 reconstruction efficiency cancel.

The observed event yields into the decay channels were corrected for acceptance using efficiencies derived from Monte Carlo simulations of the E687 apparatus.⁹ The relative branching ratio for the inclusive decay $D^0 \rightarrow K_S^0 K^+ K^-$ was determined to be $\Gamma(D^0 \rightarrow K_S^0 K^+ K^-)/\Gamma(D^0 \rightarrow K_S^0 \pi^+ \pi^-) = 0.20 \pm 0.05 \pm 0.04$, where the first error is statistical and the second is due to systematic uncertainty in Čerenkov identification and the choice of ℓ/σ_ℓ cut.¹⁰ The result is in good agreement with the world average[8] of 0.20 ± 0.05 .

The inclusive $D^0 \rightarrow K_S^0 K^+ K^-$ signal can be analyzed to extract the fraction of events into the $K_S^0 \phi$ mode. To select $D^0 \rightarrow K_S^0 \phi$ decays, events are required to have a $K^+ K^-$ invariant mass within 10 MeV/ c^2 of the nominal ϕ mass[8]. The invariant mass histogram for these candidates is shown in Fig. 5(a) and the resultant yield is

⁹The relative efficiency of the two modes is $\epsilon(K_S^0 K^+ K^-)/\epsilon(K_S^0 \pi^+ \pi^-) = 1.76 \pm 0.04$.

¹⁰The systematic uncertainty due to Čerenkov identification was estimated by comparing the efficiency derived from Monte Carlo simulations of the E687 apparatus to that derived from studies of the high statistics modes such as $D^+ \rightarrow K^- \pi^+ \pi^+$. The systematic uncertainty due to the choice of decay flight cut was obtained by evaluating the relative branching ratio over the range $\ell/\sigma_\ell > 2$ to $\ell/\sigma_\ell > 5$.

17 ± 5 events. An average of high and low mass sidebands¹¹ about the ϕ were used to estimate the contributions from other sources.¹² After the sideband subtraction, the number of $D^0 \rightarrow K_S^0 \phi$ decays was found to be 12.6 ± 5.8 events. Correcting for efficiency and the branching fraction for $\phi \rightarrow K^+ K^-$, the relative branching ratio obtained is $\Gamma(D^0 \rightarrow K_S^0 \phi) / \Gamma(D^0 \rightarrow K_S^0 \pi^+ \pi^-) = 0.13 \pm 0.06 \pm 0.02$. The systematic error reflects uncertainties in Čerenkov identification, the choice of decay flight cut, and sideband selections. Our result confirms earlier observations and is consistent with the world average[8] of 0.150 ± 0.028 .

An estimate of the $D^0 \rightarrow K_S^0(K^+ K^-)_{non-\phi}$ ratio may be obtained by excluding $K^+ K^-$ pairs which are due to $\phi \rightarrow K^+ K^-$. After requiring $M(K^+ K^-)$ to lie outside of the ϕ region one obtains 20 ± 6 events as shown in the $K_S^0 K^+ K^-$ invariant mass distribution of Fig. 5(b). For this sample a decay flight requirement of $\ell/\sigma_\ell > 4.0$ was utilized to improve the signal to background ratio. Accounting for events in the ϕ region which are not due to $D^0 \rightarrow K_S^0 \phi$, the relative branching ratio is found to be $\Gamma(D^0 \rightarrow K_S^0(K^+ K^-)_{non-\phi}) / \Gamma(D^0 \rightarrow K_S^0 \pi^+ \pi^-) = 0.11 \pm 0.04 \pm 0.03$, which is consistent with the ARGUS[2] result of 0.084 ± 0.020 .¹³

We wish to acknowledge the assistance of the staffs of Fermilab and the INFN of Italy, and the physics departments of Bologna University, University of Colorado, University of Illinois, University of Milan, Northwestern University, University of

¹¹The sidebands were chosen as $0.988 < M(K^+ K^-) < 1.008 \text{ GeV}/c^2$ and $1.050 < M(K^+ K^-) < 1.070 \text{ GeV}/c^2$.

¹²These contributions may be due to three-body non-resonant decays, or due to the decay $D^0 \rightarrow K_S^0 a_0(980)$.

¹³The authors of Ref.[2] quote $\Gamma(D^0 \rightarrow K_S^0(K^+ K^-)_{non-\phi}) / \Gamma_{tot} = (0.64 \pm 0.15 \pm 0.09)\%$ assuming $\Gamma(D^0 \rightarrow K_S^0 \pi^+ \pi^-) / \Gamma_{tot} = (7.6 \pm 0.7 \pm 0.8)\%$, which we have factored out for comparison.

Notre Dame, and Pavia University. This research was supported in part by the National Science Foundation, the U.S. Department of Energy, the Italian Istituto Nazionale di Fisica Nucleare and Ministero della Università e della Ricerca Scientifica.

TABLES

TABLE I. Dalitz plot fit results for $D^0 \rightarrow K_S^0 \pi^+ \pi^-$.

Decay mode	Amplitude Coefficient	Phase (radians)
non-resonant	0.41 ± 0.09	-2.2 ± 0.3
$K^{*-} \pi^+$	1.0 (fixed)	0.0 (fixed)
$\bar{K}^0 \rho^0$	0.39 ± 0.07	-2.4 ± 0.5

TABLE II. Decay fraction comparisons for $D^0 \rightarrow K_S^0 \pi^+ \pi^-$.

Decay mode ¹⁴	This Work ¹⁵	Mark III[6]
non-resonant	$0.26 \pm 0.08 \pm 0.05$	$0.33 \pm 0.05 \pm 0.10$
$K^{*-} \pi^+$	$0.64 \pm 0.08 \pm 0.05$	$0.56 \pm 0.04 \pm 0.05$
$\bar{K}^0 \rho^0$	$0.20 \pm 0.06 \pm 0.03$	$0.12 \pm 0.01 \pm 0.07$

¹⁴The decay fraction for each decay mode does not reflect additional branching fractions leading to the observed $K_S^0 \pi^+ \pi^-$ final state. For example, the decay fraction for $K^{*-} \pi^+$ is for $D^0 \rightarrow K_S^0 \pi^+ \pi^-$ decays where $K_S^0 \pi^-$ resonates as K^{*-} (i.e., the branching fraction for $K^{*-} \rightarrow K_S^0 \pi^-$ has not been included).

¹⁵The relative correlation coefficients between the decay fractions are: -70% (non-resonant and $K^{*-} \pi^+$), -36% (non-resonant and $\bar{K}^0 \rho^0$), and -30% ($K^{*-} \pi^+$ and $\bar{K}^0 \rho^0$).

REFERENCES

- ^a Present address: Vector Research Company, 6903 Rockledge Drive, Bethesda, MD 20817, USA.
- ^b Present address: University of North Carolina-Asheville, Asheville, NC 28804, USA.
- ^c Present address: Cinvestav-IPN, A.P. 14-740, 07000 Mexico DF, Mexico.
- ^d Present address: STX Inc., 4400 Forbes Blvd., Lanham, MD 20706, USA.
- ^e Present address: University of Colorado, Boulder, CO 80309, USA.
- ^f Present address: Vanderbilt University, Nashville, TN 37235, USA.
- ^g Present address: University of South Carolina, Columbia, SC 29208, USA.
- ^h Present address: Fermilab, Batavia, IL 60510, USA.
- ⁱ Present address: INFN - Pavia, I-27100 Pavia, Italy.
- ^j Present address: NIKHEF-H, 1009 DB, Amsterdam, The Netherlands.
- ^k Present address: University of Alabama, Tuscaloosa, AL 35487, USA.
- ^l Present address: Brandeis University, Waltham, MA 02254, USA.
- ^m Present address: University of Illinois at Urbana-Champaign, Urbana, IL 61801, USA.
- ⁿ Present address: Nevis Labs, Columbia University, Irvington, NY 10533, USA.
- ¹ See for example the following and references therein:
M. Bauer, B. Stech, M. Wirbel, *Z. Phys. C* 34 (1987) 103.
B. Yu. Blok, M.A. Shifman, *Sov. J. Nucl. Phys.* 45 (1987) 522.
L.L. Chau, H.Y. Cheng, *Phys. Rev. D* 36 (1987) 137.
- ² ARGUS Collab., H. Albrecht *et al.*, *Z. Phys. C* 33 (1987) 359.
- ³ CLEO Collab., C. Bebek *et al.*, *Phys. Rev. Lett.* 56 (1986) 1893.

- ⁴ Mark III Collab., R.M. Baltrusaitis *et al.*, Phys. Rev. Lett. 56 (1986) 2136.
- ⁵ ACCMOR Collab., S. Barlag *et al.*, Phys. Lett. B 232 (1989) 561.
- ⁶ Mark III Collab., J. Adler *et al.*, Phys. Lett. B 196 (1987) 107.
- ⁷ E687 Collab., P.L. Frabetti *et al.*, Description and Performance of the E687 Spectrometer, FER-
MILAB Pub-90/258E (1990), to be published in Nucl. Instrum. Methods.
- ⁸ Particle Data Group, J.J. Hernández *et al.*, Phys. Lett. B 239 (1990) 1.

FIGURES

FIG. 1. Invariant mass distribution for $K_S^0\pi^+\pi^-$ combinations satisfying the decay flight requirement $\ell/\sigma_\ell > 10$.

FIG. 2. Invariant mass distribution for $K_S^0\pi^+\pi^-$ combinations with the addition of secondary vertex isolation cuts.

FIG. 3. Dalitz plot and mass-squared projections for the decay $D^0 \rightarrow K_S^0\pi^+\pi^-$. In these figures the data are represented by points, and in each projection the upper histogram describes the fitted signal plus background, while the lower histogram illustrates only the background.

FIG. 4. Invariant mass distribution for $K_S^0K^+K^-$ combinations satisfying Čerenkov and vertex requirements.

FIG. 5. Invariant mass distribution for events satisfying a) the $D^0 \rightarrow K_S^0\phi$ decay hypothesis, and b) the $D^0 \rightarrow K_S^0(K^+K^-)_{non-\phi}$ decay hypothesis.

Figure 1

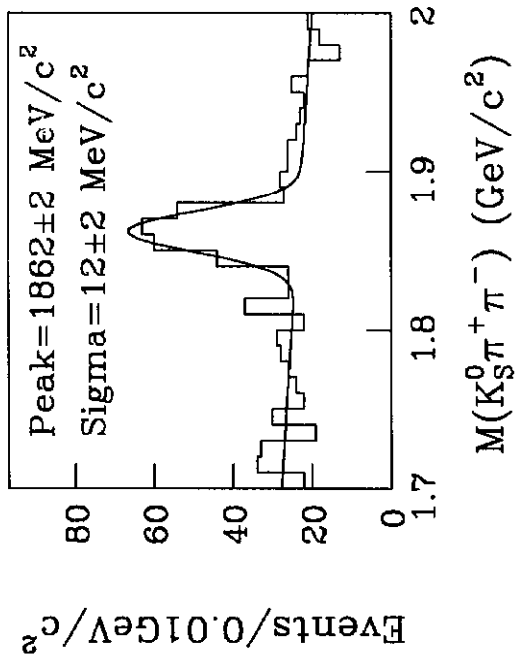
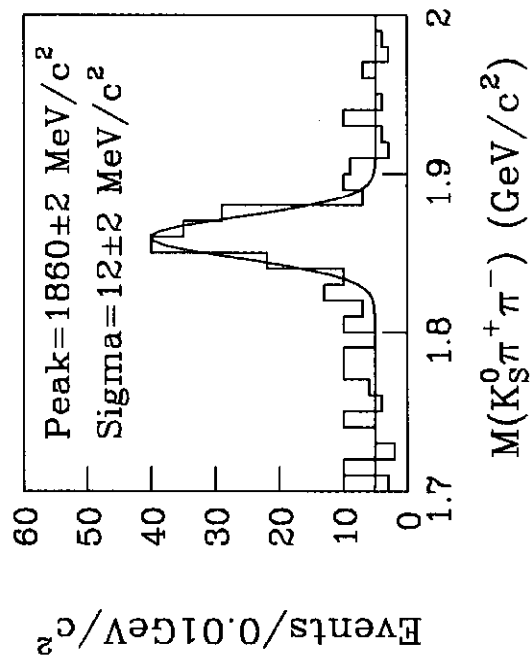


Figure 2



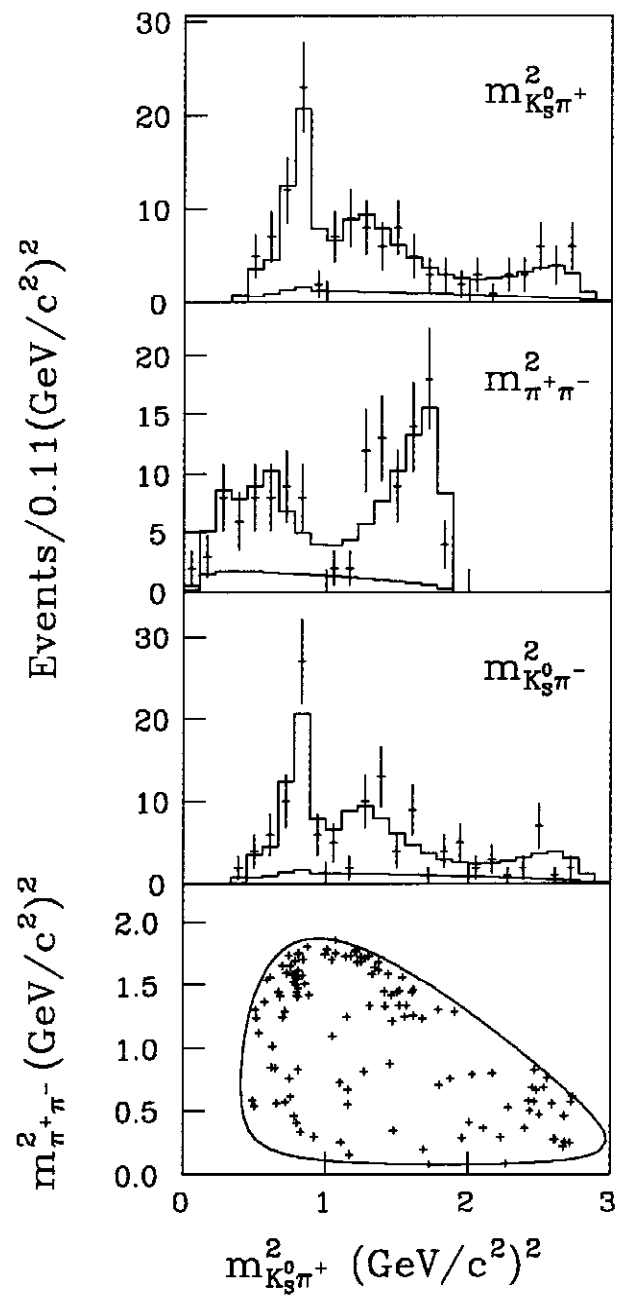


Figure 3

Figure 4

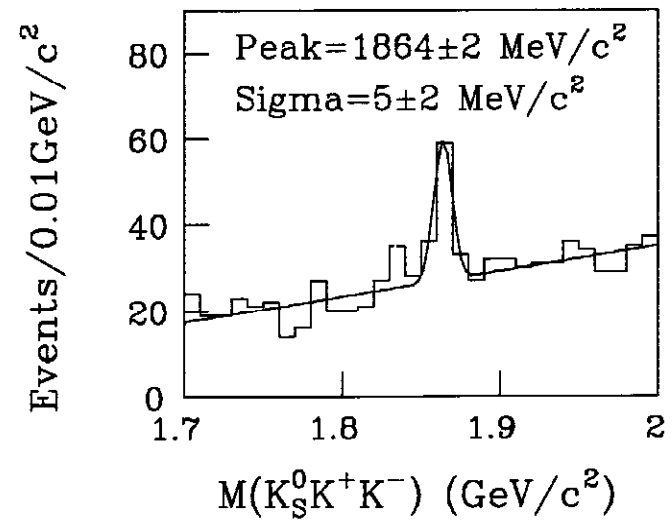


Figure 5

